Crashworthy Design of Composite Structures Using CAE Process Chain

Madhukar Chatiri[1], Thorsten Schuetz[2], Anton Matzenmiller[3]

[1]CADFEM GmbH, Grafing / Munich, Germany
[2]Adam Opel AG, GME Vehicle CAE, Ruesselsheim, Germany, thorsten.schuetz@de.opel.com

[3]Institute of Mechanics, University of Kassel, Kassel, Germany

Summary

The materials used in automotive industry should play key role in overcoming the current challenging demands such as increased global competition, need for vehicles with highest efficiency, reduction in costs, stringent environmental and safety requirements. This eventual usage of lighter materials mean lighter vehicles and low greenhouse gas emissions. Composites are getting more recognition and hence being used increasingly in the automotive industry due to their excellent weight specific characteristics such as strength and stiffness. Hence the requirements for simulations along the complete production process chain involving reinforced plastics have increased immensely. The main objective of this presentation is to present a workflow for numerical modeling and simulation of carbon fiber reinforced plastic (CFRP) composite structures including computer aided engineering (CAE) process integration. In this regard, a computational constitutive model for anisotropic damage is developed to characterize the elastic-brittle behavior of fiber-reinforced laminated composites. The presented work will introduce and discuss single steps along the process chain with in-house tools and commercial finite element program LS-DYNA®.

Keywords: CFRP, CAE process chain

1 Introduction

In the present work, a CAE process chain is described for thick and thin composite structures which consist of the following parts:
-        CAE process chain.
-        3D explicit FEA with (a) Multi-layered solid / multi-layered shell elements and (b) constitutive model wherein the damage initiation criteria are based on Puck failure criterion for first ply failure and progressive micro crack propagation is based on the idea of continuum damage evolution.

2 CAE process chain

The various manufacturing technologies of CFRP composite structures have to be represented in the finite element simulations in order to capture possible failure during production processes and exactly map the fiber orientations. CAE tool chain [1] which captures the above mentioned phenomena in manufacturing of thick composite structures (three dimensional stress state) and thin composite structures (two dimensional stress state) is explained here.

High pressure hydrogen storage system (HSS) for fuel cell vehicles with an operating pressure of 70 MPa is made of CFRP laminate with wall thickness of 40mm to 60mm. Here, three aspects are important. Firstly, the vessel has to fit into the given package space of the vehicle. Secondly, the vessel has to withstand a certain inner pressure and third, the vessel plus integration features have to pass certain vehicle crash acceptance criteria. Thus it is necessary to integrate the high pressure vessel into standard CAE processes in order to work on these aspects in the early phase of a fuel cell vehicle development. The aspect of data importing/exporting interface between individual tools, especially between the wet-winding process simulation and the FEA tools is quite efficiently done in the current tool chain (see **Fehler! Verweisquelle konnte nicht gefunden werden.**).

Starting point in the vessel pre-dimensioning phase is the given package envelope of the vehicle. This envelope defines the maximum outer dimensions of the vessel at maximum allowable working pressure. In the next step the nominal outer dimensions of the vessel are determined using an estimation of the expansion of the vessel under pressure. An iterative process is applied to determine

the required number of helical and hoop layers, the starting winding angle and the thickness of the composite. The whole iterative process considers just the cylindrical part of the vessel assuming a two dimensional state of stress and applies netting theory and classical laminate theory in a subsequent manner.
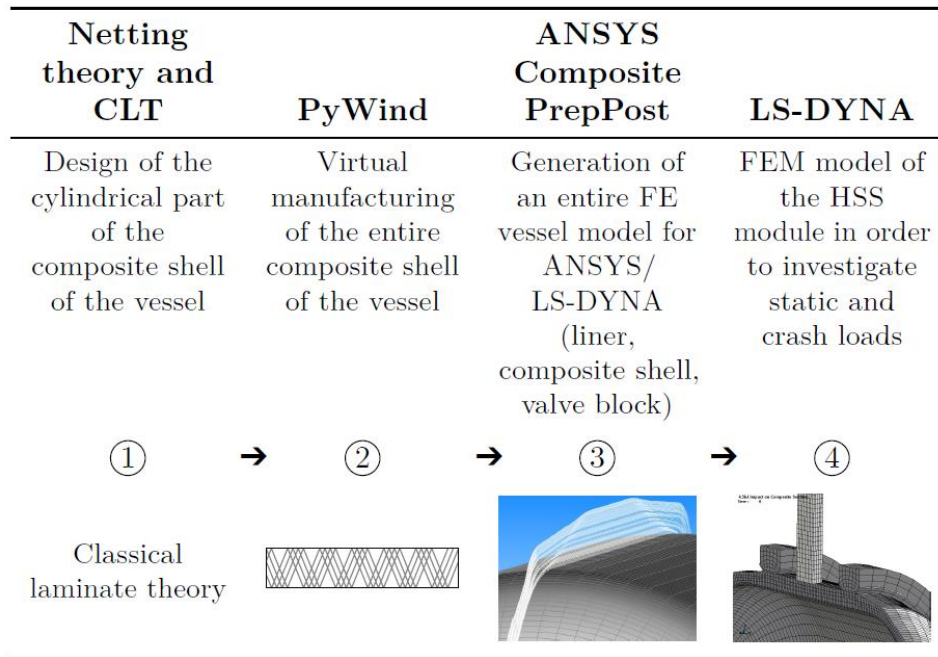
Netting theory and CLT	PyWind	ANSYS Composite PrepPost	LS-DYNA
Design of the cylindrical part of the composite shell of the vessel	Virtual manufacturing of the entire composite shell of the vessel	Generation of an entire FE vessel model for ANSYS/ LS-DYNA (liner, composite shell, valve block)	FEM model of the HSS module in order to investigate static and crash loads
① →	② →	③ →	④
Classical laminate theory			

Fig.1:   CAE process chain for thick walled composite structures.

In the next step, a detailed geometrical representation of the fiber lay-up inside the wall of a composite vessel is developed by using in-house tool Pywind. Each unidirectional (UD) layer of a composite pressure vessel is considered individually with respect to its winding angle, fiber properties and coefficient of friction.

In the third step, the Pywind data is imported inside ANSYS Composite PrepPost (ACP) and a detailed FE mesh of the wet wound composite vessel is generated. The output of the FE mesh is *ELEMENT_TSHELL_COMPOSITE [2] which allows a very comfortable description of composite layers using a ply-based concept. The FE solid model consists of a Multi-layered solid element (TSHELL type 5) which resolves the 3D stress state necessary for impact directions normal to the outer vessel surface. Also this element allows the definition of multiple integration points through the thickness in order to account for stacks of plies with arbitrary fiber orientation. In the final step, Impact and crash simulation models are generated inside LS-PrePost and simulations are done using LS-DYNA®.

The CAE process chain which is developed for thick composite structures is adapted to thin shell structures. The thin shell composite draping simulation is done using FiberSim and this data is imported inside ACP to build the composite shell structure (see Fig. 2). The output of the FE mesh is *ELEMENT_SHELL_COMPOSITE [2] which allows a very comfortable description of composite layers using a ply-based concept. Also the three dimensional material model is adapted to thin shell structures.
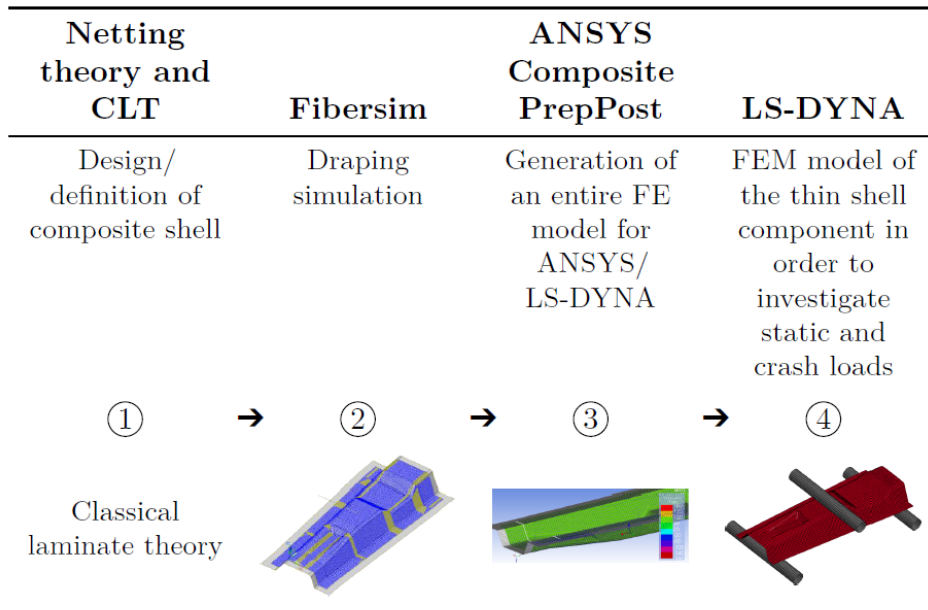
Netting theory and CLT	Fibersim	ANSYS Composite PrepPost	LS-DYNA
Design/ definition of composite shell	Draping simulation	Generation of an entire FE model for ANSYS/ LS-DYNA	FEM model of the thin shell component in order to investigate static and crash loads
① →	② →	③ →	④
Classical laminate theory			

Fig.2: CAE process chain for thin walled composite structures.

3 Constitutive modeling of composite structures

A computational constitutive model for anisotropic damage is developed to characterize the elastic-brittle behavior of fiber-reinforced laminated composites. The composite damage model is implemented within LS-DYNA® [2] as user defined material subroutine which can describe progressive failure and damage behavior of carbon fiber reinforced plastic (CFRP) composites [3]. A homogenized continuum is adopted for the constitutive theory of anisotropic damage and elasticity. Damage initiation criteria or first ply failure prediction is based on Puck failure criterion and progressive damage is based on continuum damage mechanics. Internal variables are introduced to describe the evolution of the damage state under loading and as a consequence the degradation of the material stiffness occurs. The corresponding rate equations are subjected to laws of thermomechanics. Emphasis is placed on a suitable coupling among the equations for the rates of the damage variables with respect to different damage modes. The integrated routine is successfully utilized to predict failure and damage of composite laminates which are subjected to impact conditions.

3.1 Fibre failure (FF) or longitudinal failure

Fibre fracture - see Fig. 3 (a) an 3 (b) is primarily caused by the stress σ_{11} which acts parallel to the fibres. It expresses the physical idea that fibre fracture under a multiaxial state of stress in a UD-lamina occurs when its stress parallel to the fibres σ_{11} is equal to or exceeds the stress necessary for fracture. The simple Puck FF-condition follows from this hypothesis [4, 5, and 6]. It describes by case distinction the tensile fibre mode

for $\sigma_{11} \geq 0$:
$$f_{E,FF}^{+} = \left(\frac{\sigma_{11}}{R_{\parallel}^{+}}\right)^2 - 1 \begin{cases} \geq 0 \text{ failed} \\ < 0 \text{ elastic} \end{cases} \tag{1}$$

and the compressive fibre mode

for $\sigma_{11} < 0$:
$$f_{E,FF}^{-} = \left(\frac{\sigma_{11}}{R_{\parallel}^{-}}\right)^2 - 1 \begin{cases} \geq 0 \text{ failed} \\ < 0 \text{ elastic} \end{cases} \tag{2}$$

wherein $R_{\parallel}^{+}$, $R_{\parallel}^{-}$ denote the corresponding material strength parameters.

3.2 Inter-fibre failure (IFF) or transverse failure

Normal stresses, acting transverse to the fibres and shear stresses are transmitted through both matrix and fibres. However, their damaging effect mainly takes place in the matrix or in the fibre-matrix interface, leading to debonding. Usually, the bond strength of the interface zone between fibres and matrix is the lowest in comparison to the data for the strength of the single constituents. Advancing cracks in the matrix soon pass into the fibre-matrix interface and propagate along the fibres without

crossing into the fibre material. Progressive opening of existing cracks is characteristic for tensile loading in transverse direction, whereas "crushing" in the sense of "fragmentation" of brittle matrix materials is very typical for compression in transverse direction. Following the FF, see Fig. 3 (a), 3 (b) and IFF, see Fig. 3 (c), 3 (d), 3 (e), observations outlined above, the failure modes considered in the model proposed here are schematically represented in Fig. 3.
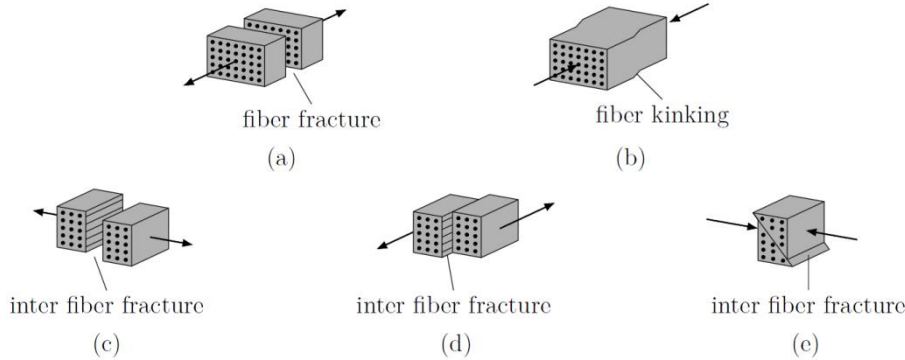

fiber fracture (a)   fiber kinking (b)

inter fiber fracture (c)   inter fiber fracture (d)   inter fiber fracture (e)

Fig. 3: Major failure modes considered in the model as in Knops [5]

For the above described transverse failure, the Puck IFF criteria are most promising for brittle, plastic unidirectional (UD-) laminates - see Fig. 4. The UD-ply behaves transversely isotropic in both cases, elasticity and failure. Puck assumes a Mohr–Coulomb type of failure criterion for loading transverse to the fibre direction. Failure is assumed to be caused by the normal and shear components operating on the action plane of stresses $\sigma_n, \tau_{n1}, \tau_{nt}$ - see Fig. 4. Positive normal stress on this plane promotes fracture while a negative one increases the material's shear strength, thus, impeding fracture. Puck's stress based failure criteria enable the computation of the material exposure $f_{E,IFF}(\theta)$ as a failure indicator, wherein θ is the orientation angle.
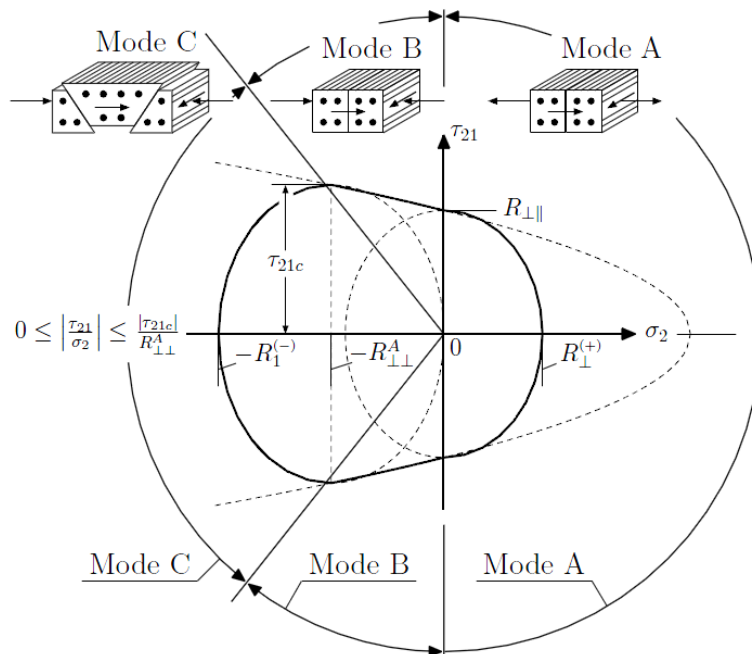

Fig. 4: Schematic representation of failure modes and failure plane based on Puck, as in [6]

The 3D Puck failure criterion can be categorized as below in Tab. 1 in extension to Fig. 4.

Table 1**:** Categorization of fracture modes in failure criteria of Puck under three dimensional stress states

Fracture angle	Sign of σ_n	Fracture mode
$90°$	positive	Delamination
$0°$ to $89°$	positive	A
$-53°$ to $0°$	negative	B
$-90°$ to $-53°$	negative	C

The values of $f_{E,IFF}(\theta)$ range between 0, where the material is unstressed, and up to 1, denoting the onset of IFF. The master failure surface on the fracture plane is defined in terms of the Mohr-Coulomb stresses, thus, yielding the following failure criteria by case distinction in tension and compression: for $\sigma_n \geq 0$:

$$f_{E,IFF}^+(\theta) = \sqrt{\left[\frac{1}{R_\perp^+} - \frac{p_{\perp\psi}^+}{R_{\perp\psi}^A}\right]^2 [\sigma_n(\theta)]^2 + \left[\frac{\tau_{nt}(\theta)}{R_{\perp\perp}^A}\right]^2 + \left[\frac{\tau_{n1}(\theta)}{R_{\perp\parallel}}\right]^2} + \frac{p_{\perp\psi}^+}{R_{\perp\psi}^A}\sigma_n(\theta) - 1 \qquad (3)$$

and
for $\sigma_n < 0$:

$$f_{E,IFF}^-(\theta) = \sqrt{\left[\frac{\tau_{nt}(\theta)}{R_{\perp\perp}^A}\right]^2 + \left[\frac{\tau_{n1}(\theta)}{R_{\perp\parallel}}\right]^2 + \left[\frac{p_{\perp\psi}^-}{R_{\perp\psi}^A}\sigma_n(\theta)\right]^2} + \frac{p_{\perp\psi}^-}{R_{\perp\psi}^A}\sigma_n(\theta) - 1 \qquad (4)$$

The only unknown parameters in these equations are $p_{\perp\psi}^\pm$, $R_{\perp\psi}^A$, and $R_{\perp\perp}^A$ which depend on the shear stresses τ_{nt} and τ_{nt} according to the following equations:

$$\frac{p_{\perp\psi}^\pm}{R_{\perp\psi}^A} = \frac{p_{\perp\perp}^\pm}{R_{\perp\perp}^A}\frac{\tau_{nt}^2}{\tau_{nt}^2 + \tau_{n1}^2} + \frac{p_{\perp\parallel}^\pm}{R_{\perp\parallel}}\frac{\tau_{n1}^2}{\tau_{nt}^2 + \tau_{n1}^2} \qquad (5)$$

and

$$R_{\perp\perp}^A = \frac{R_\perp^-}{2(1 + p_{\perp\perp}^-)} \qquad (6)$$

wherein $R_\perp^+, R_{\perp\parallel}, R_\perp^-$ denote the corresponding material strength parameters, and $p_{\perp\perp}^\pm$, $p_{\perp\parallel}^\pm$ are constants introduced by Puck, see [6]. The action plane with the greatest failure effort $f_E(\theta)$ (wherein $\theta = -90°\ to +90°$) is the fracture plane to be expected, $[f_E(\theta)]_{max} = f_E|_{\theta=\theta_{fp}}$. Once the failure plane with max $f_E(\theta)$ is found, the fracture angle as θ_{fp} is kept constant in the model and progressive failure, based on the idea of continuum damage, is applied to the material model for the corresponding lamina at hand, see below.

The failure criteria may be interpreted as loading criteria, a terminology encountered in strain space plasticity. The role played by the yield stress in plasticity will be taken by the threshold variables r_i in damage mechanics. In classical continuum damage mechanics, only the undamaged (whole) part of the cross-section A (net-area) for the uniaxial case is supposed to carry loading, i.e. transmit stresses. Consequently, the stresses σ_{ij} in the failure criteria should be interpreted as effective stresses $\hat{\sigma}_{ij}$, referred to the net area. This means that the failure criteria are assumed to hold in terms of the effective stresses rather than the nominal ones.

If the degradation is described in the sense of CAUCHY's stress concept, six different non-negative damage parameters ω_{11}, ω_{22}, ω_{33}, ω_{12}, ω_{23} and ω_{13} are defined to quantify the relative size of macro cracks projected onto the coordinate planes, and assembled in the rank-four damage operator **M** given in VOIGT notation of Eq. 8d. In CDM, the effective normal stresses $\hat{\sigma}$ are related to the damage parameters ω_{ij}, since only the undamaged part of the cross section A for the uniaxial case is

supposed to carry loading. Consequently, the stresses σ_{ij} in the failure criteria should be interpreted as effective stresses $\hat{\sigma}_{ij}$, referred to the net area. A simple relationship between effective stress $\hat{\sigma}$ and the nominal one σ holds:

$$\hat{\sigma} = \mathbf{M}\sigma \tag{7}$$

wherein $\mathbf{M}$ represents the rank-four (uncoupled) damage operator given in VOIGT notation as:

$$\sigma = \begin{bmatrix} \sigma_{11} \\ \sigma_{22} \\ \sigma_{33} \\ \tau_{12} \\ \tau_{23} \\ \tau_{13} \end{bmatrix}, \quad \hat{\sigma} = \begin{bmatrix} \hat{\sigma}_{11} \\ \hat{\sigma}_{22} \\ \hat{\sigma}_{33} \\ \hat{\tau}_{12} \\ \hat{\tau}_{23} \\ \hat{\tau}_{13} \end{bmatrix}, \quad \omega = \begin{bmatrix} \omega_{11} \\ \omega_{22} \\ \omega_{33} \\ \omega_{12} \\ \omega_{23} \\ \omega_{13} \end{bmatrix}, \quad \mathbf{M} = \begin{bmatrix} \frac{1}{1-\omega_{11}} & 0 & 0 & 0 & 0 & 0 \\ 0 & \frac{1}{1-\omega_{22}} & 0 & 0 & 0 & 0 \\ 0 & 0 & \frac{1}{1-\omega_{33}} & 0 & 0 & 0 \\ 0 & 0 & 0 & \frac{1}{1-\omega_{12}} & 0 & 0 \\ 0 & 0 & 0 & 0 & \frac{1}{1-\omega_{23}} & 0 \\ 0 & 0 & 0 & 0 & 0 & \frac{1}{1-\omega_{13}} \end{bmatrix} \tag{8a-d}$$

In the undamaged state, a lamina behaves equally in the transverse 2-direction and the through-thickness 3-direction which allows to reduce the general anisotropy to a transversely isotropic behavior with only a fiber-parallel ∥ (1) and fibre-perpendicular ⊥ (2) direction. The constitutive behavior, i.e. the material equation relating, states of stress to states of strain, is then defined by the transversely isotropic compliance matrix S in VOIGT notation for the UD-laminae prior to the damage initiation, see Eq. 9. The nonlinear behavior in-plane shear $G_{\parallel\perp}(\epsilon_{12})$ is also modeled.

$$\begin{bmatrix} \epsilon_{11} \\ \epsilon_{22} \\ \epsilon_{33} \\ 2\epsilon_{12} \\ 2\epsilon_{23} \\ 2\epsilon_{13} \end{bmatrix} = \begin{bmatrix} \frac{1}{E_{11}} & -\frac{\nu_{21}}{E_{22}} & -\frac{\nu_{31}}{E_{33}} & 0 & 0 & 0 \\ -\frac{\nu_{12}}{E_{11}} & \frac{1}{E_{22}} & -\frac{\nu_{32}}{E_{33}} & 0 & 0 & 0 \\ -\frac{\nu_{13}}{E_{11}} & -\frac{\nu_{23}}{E_{22}} & \frac{1}{E_{33}} & 0 & 0 & 0 \\ 0 & 0 & 0 & \frac{1}{G_{12}(\epsilon_{12})} & 0 & 0 \\ 0 & 0 & 0 & 0 & \frac{1}{G_{23}} & 0 \\ 0 & 0 & 0 & 0 & 0 & \frac{1}{G_{13}} \end{bmatrix} \begin{bmatrix} \sigma_{11} \\ \sigma_{22} \\ \sigma_{33} \\ \sigma_{12} \\ \sigma_{23} \\ \sigma_{13} \end{bmatrix} \tag{9}$$

The components of the constitutive tensor are represented as functions of the vector ω, comprising all internal damage variables, and the material parameters of the undamaged lamina. The constitutive tensor $\mathbf{C}(\omega)$ is derived by physical arguments and information of the dependencies between effective elastic properties and individual damage variables. Generally, for a given arbitrary damage operator, the postulate of strain equivalence yields an unsymmetrical constitutive tensor, which should be rejected as a model for the elastic behavior. This hypothesis serves here as a first guidance together with physical arguments to set up the constitutive tensor $\mathbf{C}(\omega)$ for the damaged lamina. For the purpose of building the dependence on damage into the constitutive assumption, the compliance relationship is more easily accessible in order to relate the material parameters to the mechanical response in the coordinate system with preferred axes. The compliance relationship for orthotropic elasticity in terms of effective stresses $\hat{\sigma}$ reads as:

$$\epsilon = \mathbf{H}_0\hat{\sigma}, \quad \mathbf{H}_0 = \begin{bmatrix} \frac{1}{E_{11}} & -\frac{\nu_{21}}{E_{22}} & -\frac{\nu_{31}}{E_{33}} & 0 & 0 & 0 \\ -\frac{\nu_{12}}{E_{11}} & \frac{1}{E_{22}} & -\frac{\nu_{32}}{E_{33}} & 0 & 0 & 0 \\ -\frac{\nu_{13}}{E_{11}} & -\frac{\nu_{23}}{E_{22}} & \frac{1}{E_{33}} & 0 & 0 & 0 \\ 0 & 0 & 0 & \frac{1}{G_{12}(\epsilon_{12})} & 0 & 0 \\ 0 & 0 & 0 & 0 & \frac{1}{G_{23}} & 0 \\ 0 & 0 & 0 & 0 & 0 & \frac{1}{G_{13}} \end{bmatrix}, \quad \epsilon = \begin{bmatrix} \epsilon_{11} \\ \epsilon_{22} \\ \epsilon_{33} \\ 2\epsilon_{12} \\ 2\epsilon_{23} \\ 2\epsilon_{13} \end{bmatrix} \tag{10a-c}$$

It is to be noted that Eq. (10b) is symmetric. Equations (7) and (10a) result in:

$$\epsilon = \mathbf{H}_0\hat{\sigma} = \mathbf{H}_0\mathbf{M}\sigma \tag{11}$$

The final relationship of the compliance tensor for the damaged laminae $\mathbf{H}(\boldsymbol{\omega})$ takes the following form after Poisson's ratios $\nu_{12}(\boldsymbol{\omega})$ and $\nu_{21}(\boldsymbol{\omega})$ are adjusted according to the qualitative arguments presented in [7].

$$\mathbf{H}(\boldsymbol{\omega}) = \begin{bmatrix} \frac{1}{(1-\omega_{11})E_{11}} & -\frac{\nu_{21}}{E_{22}} & -\frac{\nu_{31}}{E_{33}} & 0 & 0 & 0 \\ -\frac{\nu_{12}}{E_{11}} & \frac{1}{(1-\omega_{22})E_{22}} & -\frac{\nu_{32}}{E_{33}} & 0 & 0 & 0 \\ -\frac{\nu_{13}}{E_{11}} & -\frac{\nu_{23}}{E_{22}} & \frac{1}{(1-\omega_{33})E_{33}} & 0 & 0 & 0 \\ 0 & 0 & 0 & \frac{1}{(1-\omega_{12})G_{12}(\epsilon_{12})} & 0 & 0 \\ 0 & 0 & 0 & 0 & \frac{1}{(1-\omega_{23})G_{23}} & 0 \\ 0 & 0 & 0 & 0 & 0 & \frac{1}{(1-\omega_{13})G_{13}} \end{bmatrix} \tag{12}$$

As explained earlier, the orthotropic nature of the lamina as a homogenized continuum is maintained throughout the damaging process. The shear coupling terms are neglected. Therefore, the symmetry class of the UD-lamina remains the same for all states of damage. Its inverse always exits as long as the damage variables are less than one ($\omega_{ij} < 1$). Hence, the material stiffness tensor is given by:

$$\mathbf{C}(\boldsymbol{\omega}) = [\mathbf{H}(\boldsymbol{\omega})]^{-1}$$

3.3 Verification example

In this verification example, a tension test under loading transverse to fibre direction on a UD-reinforced laminated composite is presented. The lamina material properties for elasticity are: E_{11}=126GPa, E_{22}=11GPa, E_{33}=11GPa, ν_{12}=0.28, ν_{23}=0.40, ν_{13}=0.28, G_{12}=9GPa; and for strength: $R_{\perp}^{(+)} = 45\,\text{MPa}, R_{\perp\|} = 79\text{MPa}, R_{\|}^{(+)} = 1950\,\text{MPa}$. The load is applied in transverse (to fibre) direction until complete failure. Fig. 5 left and Fig. 5 right represents the evolution of damage variables in both original two dimensional (2D) model and the current three dimensional (3D) extension of the model for strain softening exponent $m = 1.0$. Unlike in the original two dimensional model from [7], where the damage variables effect the stress-strain curves over the entire strain range, in the current model, the damage variables are only applicable to the post-failure part.
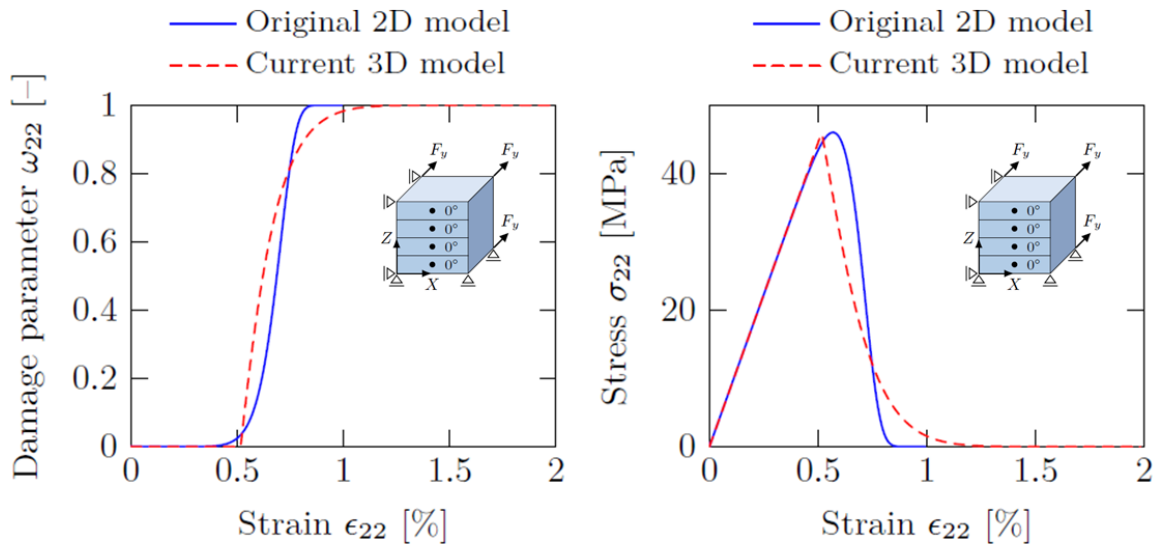

Fig. 5: left: Evolution of damage variable ω_{22} in the original 2D model and current 3D model and right: transverse stress-strain curve in both the models

3.4 Comparison with other material models inside LS-DYNA

The current user-defined material model is also tested and compared with the available material models within LS-DYNA®, see Fig. 6.
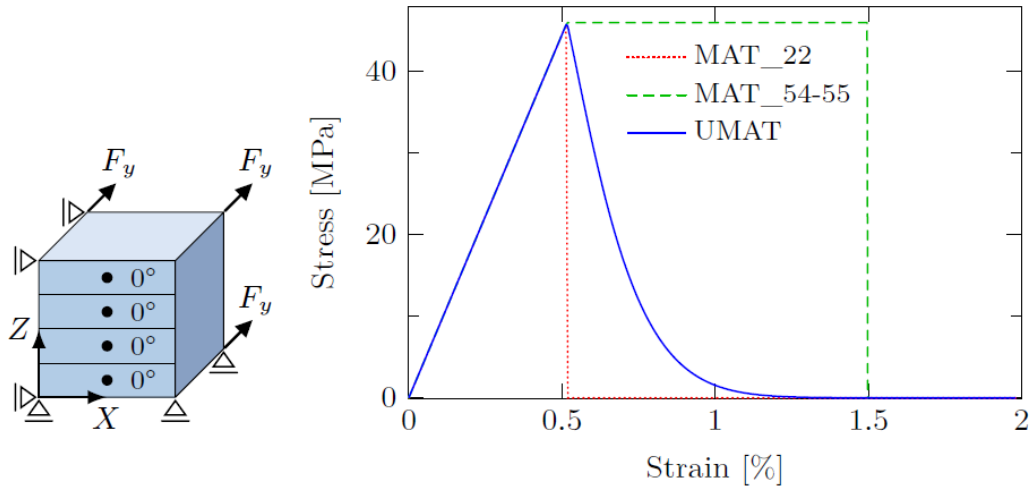

Fig. 6: Comparison of stresses with material models within LS-DYNA

3.5 Four point bending of a thick composite structure

A 4-point bending response on a laminate with configuration of ($\pm 20_2/90_4/\pm 20_2/90_4$) is shown in the below example. The material properties are taken from OPEL. The simulated model is a quarter symmetry model. Fig. 7 (left) shows the IFF predicted by Puck failure criteria and Fig. 7 (right) shows the force vs. strain results compared with experiment.
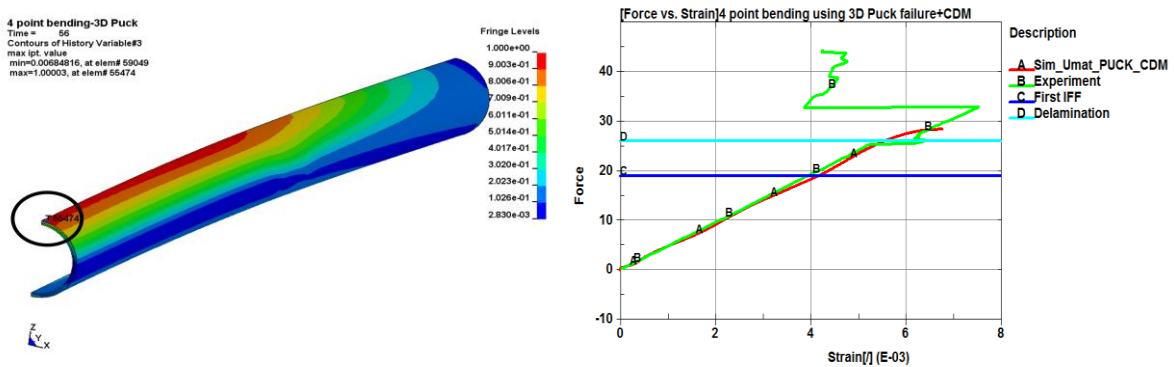

Fig. 7: left: Firs-ply failure (IFF) inside the tube using 3D puck failure criteria and right: comparison with test (strain gauge signal from tension side)

3.6 Three point bending of a thin shell structure

To check the application of the developed material model to thin shell structures, a three point bending simulation is performed on a hat profile with laminate configuration $(0/90/-45/+45)_s$. The material properties are taken from OPEL. Matrix damage and force vs. displacement are shown in the Fig. 8
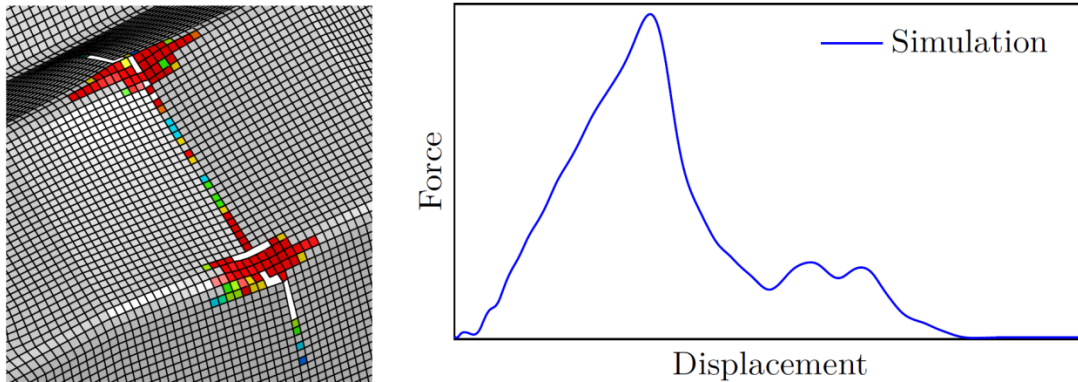
Fig. 8: 3-point bending test simulation results: Left, matrix damage and right, force vs. displacement.

4 Summary and conclusions

The CAE process chain is successfully implemented in the design phase both for thick as well as thin composite structures. The meso-level model with the 3D Puck failure criteria and anisotropic continuum damage mechanics is very effective in analyzing multi-layered structures having a large number of plies. The developed material model describes both onset and progression of damage. It can reproduce the key physical aspects observed in the failure of Fibre-reinforced laminated composite structures.

5 Literature

[1] Chatiri, M.; Schuetz, T.: Optimized design of Composite Structures Using CAE Process Chain, Nafems Seminar: Simulation of Composites - a closed process chain?, 28th – 29th . October 2014, Leipzig, Germany.

[2] Hallquist, J.O.: LS-DYNA Keyword Manual Version 971. Livermore Software Technology Corporation, Livermore, 2013

[3] Chatiri, M.; Matzenmiller, A.: A Damage-Mode Based Three Dimensional Constitutive Model for Fibre-Reinforced Composites, Computers, Materials & Continua, Vol. 35, No. 3, pp. 255-283, 2013

[4] Hashin, Z. : Failure criteria for unidirectional fibre composites, J. Appl. Mech. vol. 47, pp. 329-334, 1980

[5] Knops, M.: Analysis of Failure in Fibre Polymer Laminates: The Theory of Alfred Puck. Springer-Verlag: Berlin, Heidelberg, 2008

[6] Puck, A.; Schürmann, H. : Failure analysis of FRP laminates by means of physically based phenomenological models, in Failure Criteria in Fibre Reinforced Polymer Composites: The World-Wide Failure Exercise, P. D. Hinton, A. S. Kaddour, and M. L. Soden, Eds. Elsevier: Oxford, pp. 832-876, 2004

[7] Matzenmiller, A.; Lubliner, J.; Taylor, R. L.: A constitutive model for anisotropic damage in fibre composites, Mechanics of Materials, vol. 20, pp. 125-152, 1995